Dyes and Pigments 92 (2012) 1292–1299

Contents lists available at SciVerse ScienceDirect

Dyes and Pigments

journal homepage: www.elsevier.com/locate/dyepig

Organic dyes incorporating the cyclopentadithiophene moiety for efficient dye-sensitized solar cells

Xiaobing Cheng, Siyuan Sun, Mao Liang*, Yongbo Shi, Zhe Sun, Song Xue*

Department of Applied Chemistry, Tianjin University of Technology, Tianjin 300384, PR China

ARTICLE INFO

Article history:
Received 28 April 2011
Received in revised form
15 August 2011
Accepted 22 September 2011
Available online 1 October 2011

Keywords:
Dye-sensitized solar cell
Organic dye
Triarylamine
Cyclopentadithiophene
Conjugated bridge
Photovoltaic

ABSTRACT

Three triarylamine organic dyes (**XS28**–**30**) containing a cyclopentadithiophene unit as the conjugated bridge have been designed and synthesized for a potential application in dye-sensitized solar cells (DSSCs). Their absorption spectra, electrochemical and photovoltaic properties have been investigated. The incorporation of ethyl-substituted cyclopentadithiophene is highly beneficial to light-harvesting and preventing close π–π aggregation, thus favorably generating high efficiency. For a typical device, a solar energy conversion efficiency (η) of 5.8% based on **XS29** was achieved under simulated AM 1.5 solar irradiation (100 mW cm^{-2}) with a short-circuit photocurrent density (J_{SC}) of 14.4 mA cm^{-2}, an open-circuit voltage (V_{OC}) of 601 mV, and a fill factor (ff) of 0.68. These results suggest that the functionalized cyclopentadithiophene unit is a promising candidate for DSSCs.

1. Introduction

Recently, dye-sentsitized solar cells (DSSCs), considered as a credible alternative to conventional inorganic silicon-based solar cells, have attracted much attention relevant to global environmental issues [1]. It has been found that the nature of photosensitizers, such as redox potential, structure and photophysical properties, etc., play an important role in determining the overall cell efficiencies. To date, two kinds of photosensitizers, ruthenium dyes [2,3] and metal-free organic dyes, were developed for DSSCs. Metal-free organic dyes were regarded as an alternative to ruthenium dyes owing to their high molar absorption coefficient, simple synthesis procedure, and low cost. Various kinds of metal-free organic dyes such as coumarin- [4–6], indoline- [7–10], triphenylamine- [11–19], phenothiazine- [20], dimethylfluorene- [21], truxene- [22–25], merocyanine- [26], hemicyanine- [27] and carbazole- [28] have been investigated as sensitizers for DSSCs.

By far the most common investigated organic dyes are usually composed by an electron donor (D), a conjugated bridging segment (π), and an electron acceptor (A). This D–π–A dipolar architecture produces an effective intramolecular charge transfer from D to A during photoexcitation. Aside from the electron donor and electron acceptor in a typical push–pull dye, the conjugated bridging segment is widely recognized of its significance for performance control of DSSCs [29]. Organic dyes based on thiophene, oligothiophene moiety [28], 3,4-ethylenedioxythiophene (EDOT) [12], thieno[3,2-b]thiophene (TT) [30] and dithieno[3,2-*b*:2′,3′-*d*] thiophene (DTT) [31] as efficient bridging segments have been reported, showing high values of the overall conversion efficiencies.

Cyclopentadithiophene, emerged as a attractive building block for the development of conducting materials [32], has attracted our interest for design of photosenzitizers due to its special properties of rigid conjugation structure and facile introduction of alkyl chains. Organic dyes using the alkyl-functionalized cyclopentadithiophene as the conjugated bridge segment are expected to improve optical properties, suppress dye aggregation, and retard charge recombination. In this study, we report on the synthesis, characterization, and photovoltaic properties of three new organic dyes (**XS28**–**30**, Scheme 1), which contain functionalized 4,4-diethyl-cyclopenta(2,1-b:3,4-b′)dithiophenes moiety as the conjugated bridge. Moreover, we perform density functional theory (DFT) and time-depended density functional theory (TD-DFT) calculations to provide a detailed characterization of the structural and optical properties of the three sensitizers.

* Corresponding authors. Tel.: +86 22 60214250; fax: +86 22 60214252.
E-mail addresses: liangmao717@126.com (M. Liang), xuesong@ustc.edu.cn (S. Xue).

0143-7208/$ – see front matter © 2011 Elsevier Ltd. All rights reserved.
doi:10.1016/j.dyepig.2011.09.019

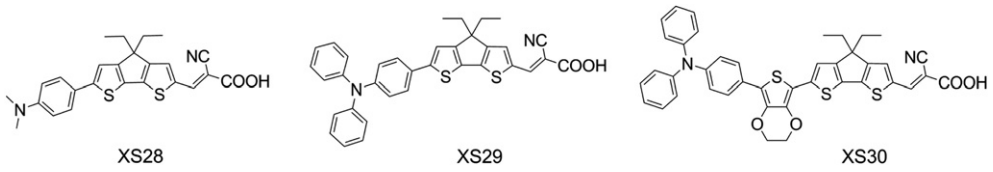

Scheme 1. Structure of organic dyes (**XS28**–**30**).

2. Experimental sections

2.1. Materials and instruments

The synthetic routes of the **XS28**–**30** dyes are shown in Scheme 2. *N*,*N*-Dimethylformamide was dried over and distilled from CaH_2 under an atmosphere of nitrogen. Phosphorus oxychloride was freshly distilled before use. Titanium (IV) isopropoxide, tertbutylpyridine and lithium iodide were purchased from Aldrich. All other solvents and chemicals used in this work were analytical grade and used without further purification.

^{1}H NMR and ^{13}C NMR spectra were recorded on a Bruker AM-400 spectrometer. The reported chemical shifts were against TMS. Mass spectra were recorded on a LCQ AD (Thermofinnigan, USA) mass spectrometer. The melting point was taken on a RY-1 thermometer and temperatures were uncorrected.

2.2. Photophysical and electrochemical measurements

The absorption spectra of the dyes either in solution or on the adsorbed TiO_2 films were measured by HITACHI U-3310 spectrophotometer. Adsorption of the dye on the TiO_2 surface was done by soaking the TiO_2 electrode in a mixture solution ethanol-dichloromethane 3:1 solution of the dye (standard concentration 3×10^{-4} M) at room temperature for 24 h. Fluorescence measurement was carried with a HITACHI F-4500 fluorescence spectrophotometer. FT-IR spectra were obtained with a Bio-Rad FTS 135 FT-IR instrument.

Cyclic voltammetry measurements were performed at room temperature on a computer controlled LK2005A electrochemical workstation with Pt-wires as working electrode and counter electrode, Ag/AgCl electrode as reference electrode with a scan rate of 100 mV s^{-1}. Tetrabutylammonium perchlorate (TBAP, 0.1 mol/L) and acetonitrile were used as supporting electrolyte and solvent, respectively. The measurements were calibrated using ferrocene as standard. The redox potential of ferrocene internal reference is taken as 0.63 V vs NHE.

2.3. Fabrication of DSSCs

The TiO_2 paste used for the preparation of the nanocrystalline films consists of 18 wt.% TiO_2, 9 wt.% ethyl cellulose and 73 wt.% terpineol [33], which was printed on a conducting glass (Nippon Sheet Glass, Hyogo, Japan, fluorine-doped SnO_2 over layer, sheet resistance of 10 Ω/sq) using a screen printing technique. The thickness of the TiO_2 film was controlled by selection of screen mesh size and repetition of printing. The film was dried in air at 120 °C for 30 min and calcined at 500 °C for 30 min under flowing oxygen before cooling to room temperature. The heated electrodes were impregnated with a 0.05 M titanium tetrachloride solution in a water-saturated desiccator at 70 °C for 30 min and fired again to give a ca. 12 μm thick mesoscopic TiO_2 film. The TiO_2 electrode was stained by immersing it into a dye solution containing 300 μM dye sensitizers (ethanol-dichloromethane 3:1) for 48 h at room temperature. Then the sensitized-electrode was rinsed with dry ethanol and dried by a dry air flow. Pt catalyst was deposited on the

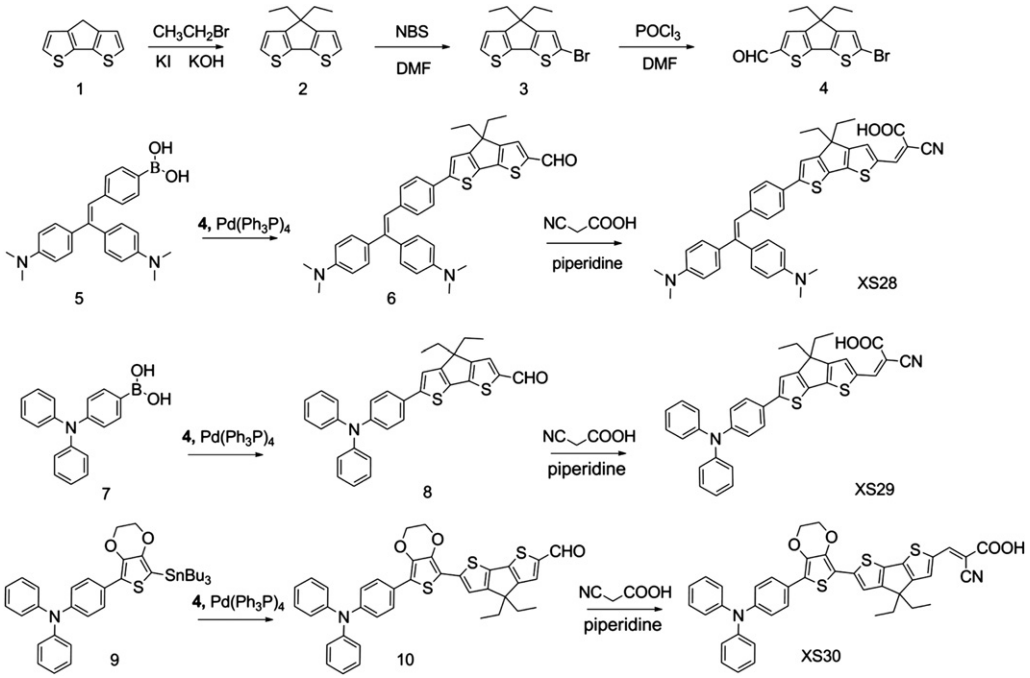

Scheme 2. Synthesis of organic dyes (**XS28**–**30**).

FTO glass by coating with a drop of H_2PtCl_6 solution (40 mM in ethanol) with the heat treatment at 395 °C for 15 min to give photoanode. The dye-covered TiO_2 electrode and Pt-counter electrode were assembled into a sandwich type cell according to the literature method [33]. The DSSCs had an active area of 0.16 cm^2 and electrolyte composed of 0.6 M 1,2-dimethyl-3-*n*-propylimidazolium iodide (DMPImI), 0.1 M LiI, 0.05 M I_2, and 0.5 M tertbutylpyridine in acetonitrile.

2.4. Characterization of DSSCs

The photocurrent–voltage (*J–V*) characteristics of the solar cells were carried out using a Keithley 2400 digital source meter controlled by a computer and a standard AM1.5 solar simulator-Oriel 91160-1000 (300 W) SOLAR SIMULATOR 2 × 2 BEAM. The light intensity was calibrated by an Oriel reference solar cell. The action spectra of monochromatic incident photon-to-current conversion efficiency (IPCE) for solar cell were performed by using a commercial setup (QTest Station 2000 IPCE Measurement System, CROWNTECH, USA).

2.5. Computational methods

The geometrical structures of the three dyes were optimized by performed density functional theory (DFT) calculations and time-dependent DFT (TDDFT) calculations of the excited states at the B3LYP/6-31 + G(d) level with the Gaussian 03W program package.

2.6. The detailed experimental procedures and characterization data

2.6.1. 4,4-Diethyl-4H-cyclopenta(2,1-b:3,4-b′)dithiophene (**2**)

Compound **1** (2.0 g, 11.2 mmol) was dissolved in dimethyl sulfoxide (50 mL). Bromoethane (2.4 g, 22.4 mmol) and potassium iodide (50 mg) were added. The mixture was flushed with nitrogen and cooled in an ice bath, and finely ground potassium hydroxide (2.0 g) was added in portions. The resulting green mixture was vigorously stirred overnight at room temperature. The reaction was then cooled in an ice bath, and water (50 mL) was added. The organic phase was extracted twice with ethyl acetate, washed with water and brine. The organic phase was dried with magnesium sulfate. The title compound was purified by chromatography to give an oil (2.23 g, 85%). IR (KBr): 1636, 1558, 1173, 788 cm^{-1}. ^1H NMR (400 MHz, $CDCl_3$): δ 7.20 (d, $J = 4.4$ Hz, 2H), 6.98 (d, $J = 4.4$ Hz, 2H), 1.94 (q, $J = 7.2$ Hz, 4H), 0.65 (t, $J = 7.2$ Hz, 6H). ^{13}C NMR (100 MHz, $CDCl_3$): δ 157.4, 136.9, 124.5, 121.6, 54.3, 30.1, 9.1. HRMS (ESI) calcd for $C_{13}H_{14}S_2$ ($M + H^+$): 235.0610, found: 235.0608.

2.6.2. 2-Bromo-4,4-diethyl-4H-cyclopenta(2,1-b:3,4-b′)dithiophene (**3**)

Compound **2** (1.96 g, 8.34 mmol) and NBS (1.48 g, 8.34 mmol) were dissolved in DMF (50 mL). After stirring at room temperature for 24 h, the mixture was poured into water (50 mL) and led to precipitate yellow solid. The precipitate was filtered and purified by chromatography on silica gel (petroleum: ethyl acetate = 10: 1 as eluent) to give a yellow solid (2.35 g, 90%). Mp: 47–49 °C. IR (KBr): 1636, 1558, 1138, 787 cm^{-1}. ^1H NMR (400 MHz, $CDCl_3$): δ 7.18 (s, 1H), 6.96 (d, $J = 5.6$ Hz, 2H), 1.85–1.92 (m, 4H), 0.61 (t, $J = 7.2$ Hz, 6H). ^{13}C NMR (100 MHz, $CDCl_3$): δ 156.6, 155.2, 136.8, 125.0, 124.5, 121.5, 111.1, 110.5, 55.2, 30.1, 29.6, 9.0, 8.9. HRMS (ESI) calcd for $C_{13}H_{13}BrS_2$ ($M + H^+$): 312.9715, found: 312.9708.

2.6.3. 6-Bromo-4,4-diethyl-4H-cyclopenta(2,1-b:3,4-b′) dithiophene-2-carbaldehyde (**4**)

To a solution of compound **3** (2 g, 6.36 mmol) in anhydrous DMF (12 mL, 152 mmol) at 0 °C under N_2 atmosphere was added $POCl_3$ (3.75 mL, 25 mmol) dropwise and stirred for 1 h. Subsequently, the mixture was heated at 50 °C for 12 h. The mixture was cooled and poured into an ice-water with vigorous stirring. After neutralization with NaOH, the mixture was further stirred at 70 °C for 1 h. After cooling and extraction with ethyl acetate, the organic fractions were combined and dried over with $MgSO_4$. The resulting solid was purified by column chromatography on silica gel (petroleum: ethyl acetate = 5: 1 as eluent) to give a black oil (1.42 g, 65.4%). IR (KBr): 1637, 1555, 1141, 788 cm^{-1}. ^1H NMR (400 MHz, $CDCl_3$): δ 9.85 (s, 1H), 7.57 (s, 1H), 7.03 (s, 1H), 1.97–1.92 (m, 4H), 0.62 (t, $J = 7.2$ Hz, 6H). ^{13}C NMR (100 MHz, $CDCl_3$): δ 182.4, 160.4, 156.4, 147.0, 143.6, 136.3, 129.7, 124.9, 116.2, 55.6, 29.9, 8.9. HRMS (ESI) calcd for $C_{14}H_{13}BrOS_2$ ($M + H^+$): 340.9664, found: 340.9661.

2.6.4. Synthesis of compound **6**

A mixture of compound **5** (0.183 g, 1.1 mmol), **4** (0.342 g, 1 mmol), $Pd(PPh_3)_4$ (50 mg, 0.042 mmol), aqueous 1 M Na_2CO_3 (3 mL), and 10 mL DME was refluxed for 18 h under N_2. Ethyl acetate was added before cooling down to room temperature. The organic layer was separated and washed 3 times with water, dried over anhydrous $MgSO_4$, and filtered. After removing the solvent, the resulting solid was purified by column chromatography on silica gel (petroleum: ethyl acetate = 5: 1 as eluent) as a yellow powder (0.29 g, 75%). Mp: 167–169 °C, IR (KBr): 1647, 1066, 952 cm^{-1}. ^1H NMR (400 MHz, $CDCl_3$): δ 9.80 (s, 1H), 7.53 (s, 1H), 7.51 (d, $J = 8.4$ Hz, 2H), 7.04 (s, 1H), 6.73 (d, $J = 8.4$ Hz, 2H), 3.01 (s, 6H), 1.96–1.93 (m, 4H), 0.64 (t, $J = 7.3$ Hz, 6H). ^{13}C NMR (100 MHz, $CDCl_3$): δ 182.2, 163.1, 156.2, 151.0, 150.4, 149.1, 142.3, 132.9, 129.8, 126.6, 122.7, 115.3, 112.4, 55.0, 40.3, 30.1, 9.1. HRMS (ESI) calcd for $C_{22}H_{23}NOS_2$ ($M + H^+$): 382.1272, found: 382.1283.

2.6.5. Synthesis of ***XS28***

To a solution of compound **6** (0.176 g, 0.5 mmol) and cyanoacetic acid (0.084 g, 1 mmol) in acetonitrile (10 mL) was added dichlormethane (5 mL) and piperidine (50 μL). The solution was refluxed for 24 h. After cooling the solution, the solvent was removed in vacuo. The pure product was obtained by silica gel chromatography (CH_2Cl_2: MeOH = 5: 1 as eluent) as a red powder (0.15 g, 68%). Mp: 164–167 °C. IR (KBr): 3565, 2357, 1633, 1506, 903 cm^{-1}. ^1H NMR (400 MHz, DMSO-d_6): δ 8.28 (s, 1H), 7.79 (s, 1H), 7.54 (d, $J = 8.4$ Hz, 2H), 7.41 (s, 1H), 6.77 (d, $J = 8.4$ Hz, 2H), 2.96 (s, 6H), 1.92 (q, $J = 7.2$ Hz, 4H), 0.57 (t, $J = 7.2$ Hz, 6H). ^{13}C NMR (100 MHz, DMSO-d_6): δ 165.0, 156.6, 150.6, 136.3, 132.4, 129.1, 126.6, 122.2, 116.3, 112.8, 54.8, 44.1, 29.7, 9.4. HRMS (ESI) calcd for $C_{25}H_{24}N_2O_2S_2$ ($M + H^+$): 449.1352, found: 449.1341.

2.6.6. Synthesis of compound **8**

A mixture of compound **7** (0.317 g, 1.1 mmol), **4** (0.342 g, 1 mmol), $Pd(PPh_3)_4$ (50 mg, 0.042 mmol), aqueous 1 M Na_2CO_3 (3 mL), and 10 mL DME was refluxed for 18 h under N_2. Ethyl acetate was added before cooling down to room temperature. The organic layer was separated and washed three times with water, dried over anhydrous $MgSO_4$, and filtered. After removing the solvent, the resulting solid was purified by column chromatography on silica gel (petroleum: ethyl acetate = 5: 1 as eluent) as a yellow powder (0.303 g, 60%). Mp: 198–199 °C, IR (KBr): 1638, 1141, 1066, 950 cm^{-1}. ^1H NMR (400 MHz, $CDCl_3$): δ 9.82 (s, 1H), 7.55 (s, 1H), 7.50 (d, $J = 7.9$ Hz, 2H), 7.30–7.22 (m, 5H), 7.14–7.12 (m, 5H), 7.08–7.06 (m, 3H), 1.99–1.93 (m, 4H), 0.66 (t, $J = 7.2$ Hz, 6H). ^{13}C NMR (100 MHz, $CDCl_3$): δ 182.4, 162.9, 156.7, 149.6, 148.6, 147.9, 147.3, 142.9, 134.2, 129.7, 129.4, 129.1, 128.2, 126.4, 126.3, 124.7, 123.4,

116.7, 55.1, 30.1, 9.1. HRMS (ESI) calcd for $C_{32}H_{27}NOS_2$ ($M+H^+$): 506.1607, found: 506.1589.

*2.6.7. Synthesis of **XS29***

The product was synthesized according to the procedure for the synthesis of **XS28**, giving a red powder in 70% yield. Mp: 203–205 °C. IR (KBr): 3566, 2357, 1634, 1506, 914 cm^{-1}. ^1H NMR (400 MHz, DMSO-d_6): δ 8.26 (s, 1H), 7.72 (s, 1H), 7.59 (d, $J = 8.0$ Hz, 2H), 7.49 (s, 1H), 7.35–7.30 (m, 4H), 7.10–7.03 (m, 6H), 6.98 (d, $J = 8.0$ Hz, 2H), 1.92 (d, $J = 7.2$ Hz, 4H), 0.51 (t, $J = 7.2$ Hz, 6H). ^{13}C NMR (100 MHz, DMSO-d_6): δ 165.2, 162.4, 157.1, 148.2, 147.5, 147.3, 145.2, 143.7, 137.4, 134.3, 130.1, 128.5, 126.7, 124. 8, 124.0, 123.5, 119.6, 118.2, 55.0, 29.8, 9.4. HRMS (ESI) calcd for $C_{35}H_{28}N_2O_2S_2$ ($M+H^+$): 573.1665, found: 573.1652.

*2.6.8. Synthesis of compound **10***

To a solution of compound **9** (650 mg, 0.96 mmol) and **4** (300 mg, 0.88 mmol) in toluene (15 mL), $Pd(PPh_3)_4$ (50 mg) was added. The mixture was refluxed for 6 h under argon. The crude compound was extracted into ethyl acetate, washed with brine and water, and dried over anhydrous sodium sulfate. After removing solvent under reduced pressure, the residue was purified by column chromatography (petroleum: ethyl acetate = 10: 1 as eluent) on silica gel to yield a red powder (0.352 g, 62%). Mp: 208–210 °C. IR (KBr): 1653, 1493, 1397, 1311, 1083 cm^{-1}. ^1H NMR (400 MHz, DMSO-d_6): δ 9.79 (s, 1H), 7.59 (d, $J = 8.7$ Hz, 2H), 7.52 (s, 1H), 7.27–7.23 (m, 4H), 7.12–7.02 (m, 9H), 4.41–4.34 (m, 4H), 1.94 (m, 4H), 0.63 (t, $J = 7.2$ Hz, 6H). ^{13}C NMR (100 MHz, DMSO-d_6): δ 182.3, 162.2, 156.7, 148.6, 147.4, 146.6, 142.7, 140.2, 138.7, 137.6, 134.2, 129.9, 129.3, 126.8, 126.5, 124.5, 123.4, 123.1, 116.5, 109.7, 65.0, 64.7, 55.0, 30.1, 9.0. HRMS (ESI) calcd for $C_{38}H_{31}NO_3S_3$ ($M+H^+$): 646.1466, found: 646.1462.

*2.6.9. Synthesis of **XS30***

The product was synthesized according to the procedure for the synthesis of **XS28**, giving a red powder of the product in 70% yield. Mp: >300 °C. IR (KBr): 3435, 1587, 1497, 1363, 1263, 1083 cm^{-1}. ^1H NMR (400 MHz, DMSO-d_6): δ 8.1 (s, 1H), 7.58 (d, $J = 8.7$ Hz, 2H), 7.33–7.29 (m, 5H), 7.09–6.99 (m, 9H), 4.45–4.40 (m, 4H), 1.94–1.92 (m, 4H), 0.86 (t, $J = 7.2$ Hz, 6H). ^{13}C NMR (100 MHz, DMSO-d_6): δ 162.3, 156.2, 148.8, 147.3, 143.7, 141.3, 138.3, 135.2, 130.0, 129.6, 127.1, 124.6, 123.8, 123.6, 118.5, 110.3, 65.6, 64.8, 55.2, 29.8, 9.0. HRMS (ESI) calcd for $C_{41}H_{32}N_2O_4S_3$ ($M+H^+$): 713.1524, found: 713.1522.

3. Results and discussion

3.1. UV–vis absorption/emission spectra

The UV–vis and emission spectra of the dyes **XS28**–**30** in $CHCl_3$ are displayed in Fig. 1. The characteristic data are summarized in Table 1. All the dyes display two strong absorption bands at around 300–350 nm and 400–600 nm, which mainly stem from the intramolecular charge-transfer transition. The maximum absorption peaks of **XS28**–**30** display at 521, 491, and 514 nm with molar extinction coefficient (ε) of 34 000, 36 000, and 42 000 M^{-1} cm^{-1}, respectively. **XS28** possessed of *N,N*-dimethylaniline as donor shifts the absorption peak bathochromically 30 nm compared to **XS29** with triphenylamine as donor, indicating *N,N*-dimethylaniline acted as donor unit favors the light harvesting. **XS30** bearing 3,4-ethyldioxythiophene and cyclopentadithiophene as binary spacer shows obviously red-shifted absorption compared with **XS29** due to the extension of the π-conjugation. Emission maxima of the dyes **XS28**–**30** can be found at 500 to 700 nm when the dyes are excited at their respective absorption bands at 400–600 nm.

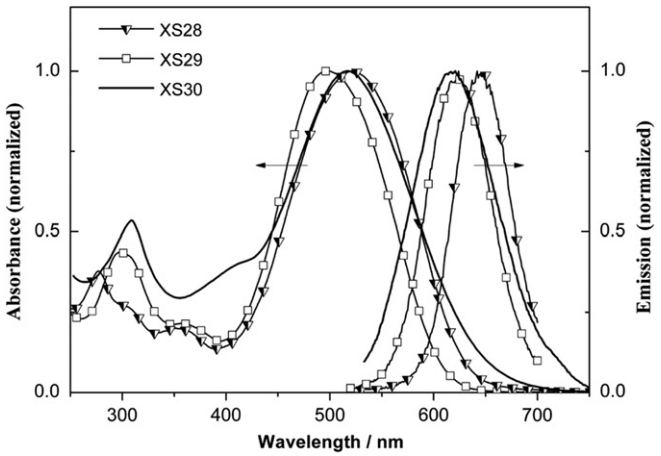

Fig. 1. Absorption and emission spectra of dyes **XS28**–**30** in $CHCl_3$ (1×10^{-5} M).

Fig. 2 shows absorption spectra of the **XS28**–**30** adsorbed on the surface of transparent mesoporous TiO_2 films (3 μm, Fig. 2a; 12 μm, Fig. 2b). Absorption of the blank TiO_2 film was subtracted from the curve. Compared to the solution spectra of **XS28**–**30**, an evident hypsochromic effect can be found for the dyes deprotonation concomitant with the carboxylate grafting of sensitizers on TiO_2 film (3 μm), which could be ascribed to a weaker electron-withdrawing capability of the carboxylatetitanium assembly than that of the carboxylic acid. It is clearly demonstrated from Fig. 2b that the absorption spectra of those adsorbed onto the similar thickness of TiO_2 films under the DSSC fabrication condition show a markedly broad profile, which is beneficial to light-harvesting.

To gain insight into the geometrical, electronic, and optical properties of the dyes **XS28**–**30**, DFT calculations and time-dependent DFT (TDDFT) calculations of the excited states were performed. The molecular structures of **XS28**–**30** are optimized in the vacuo, and the isodensity surface plots of HOMO (the highest occupied molecular orbital) and LUMO (the lowest unoccupied molecular orbital) are presented in Fig. 3. The TDDFT calculations show that the lowest excitation of three dyes is a charge-transfer transition of dominantly HOMO–LUMO character. Excitation energies and oscillator strengths (f) for dyes **XS28**–**30** are summarized in Table 2. The HOMO orbital of **XS28**–**30** is of π-character and is delocalized over the entire molecule with maximum components on the *N,N*-dimethylaniline/triphenylamine units. The LUMO orbital is, on the other hand, a single π^* orbital delocalized across the cyclopentadithiophene and cyanoacrylic acid groups with sizable contributions from the latter. This distribution of HOMO and LUMO levels is separated in the molecule of compound, indicating that transition from HOMO to LUMO can be considered as a charge-transfer transition [34]. In addition, this

Table 1
Optical properties and electrochemical properties of four dyes.

Dye	λ_{max}/nm ($\varepsilon/10^3$ M^{-1} cm^{-1})[a]	λ_{int}/nm[b]	E_{0-0}/eV[c]	E_{ox}/V[d]	E_{red}/V[e]
XS28	276 (18), 521(34)	605	2.04	0.77	−1.23
XS29	294 (19), 491(36)	576	2.15	0.91	−1.34
XS30	305 (22), 519 (42)	576	2.15	0.74	−1.40

[a] The maximum absorption peaks of dyes measured in $CHCl_3$.
[b] The intersect of the normalized absorption and the emission spectra.
[c] E_{0-0} values were calculated from intersect of the normalized absorption and the emission spectra (λ_{int}): $E_{0-0} = 1240/\lambda_{int}$.
[d] E_{ox} (vs NHE) of the dyes in acetonitrile were measured with cyclic voltammogram.
[e] E_{ox^*} (vs. NHE) was calculated from $E_{ox^*} = E_{ox} - E_{0-0}$.

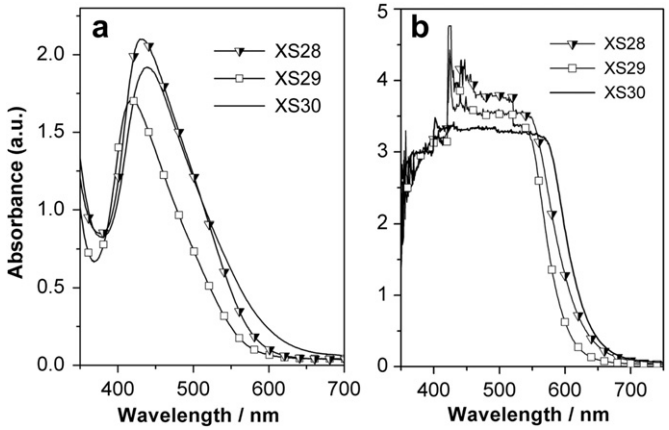

Fig. 2. Absorption spectra of **XS28**–**30** on TiO_2 transparent films (a: 3 μm; b: 12 μm).

spatially directed separation of HOMO and LUMO is an ideal condition for dye-sensitized solar cells, which not only facilitates the ultrafast interfacial electron injection but also slows down the recombination of the injected electron with the oxidized dyes.

3.2. Electrochemical properties

To obtain and understand the molecular orbital energy levels, cyclic voltammetry (CV) was employed to measure the ground-state oxidation potential (E_{ox}) of the dyes in acetonitrile solution. Representative cyclic voltammograms are shown in Fig. 4. The corresponding electrochemistry data are given in Table 2. **XS28**–**30** exhibit two reversible processes in the oxidation scan. The first quasi-reversible one-electron oxidation wave is attributed to the removal of electron from the *N*,*N*-dimethylaniline/triphenylamine unit. The second quasi-reversible one-electron oxidation wave at a higher potential is attributed to the oxidation of cyclopentadithiophene/EDOT-cyclopentadithiophene since oligothienyl ring is a potent electron donor.

For the three dyes, the first oxidation potential at the ground state is taken as the highest occupied molecular orbital (HOMO) level. The excited-state potential (E_{ox^*}), reflecting the LUMO level of the dye, can be derived from the ground-state oxidation potential (E_{ox}) and the zero–zero excitation energy (E_{0-0}) according to the following equation: $E_{ox^*} = E_{ox} - E_{0-0}$. As depicted in Table 1, the HOMO levels of the dyes **XS28**–**30** are 0.77, 0.91, and 0.74 V vs NHE, respectively. The LUMO levels of the dyes

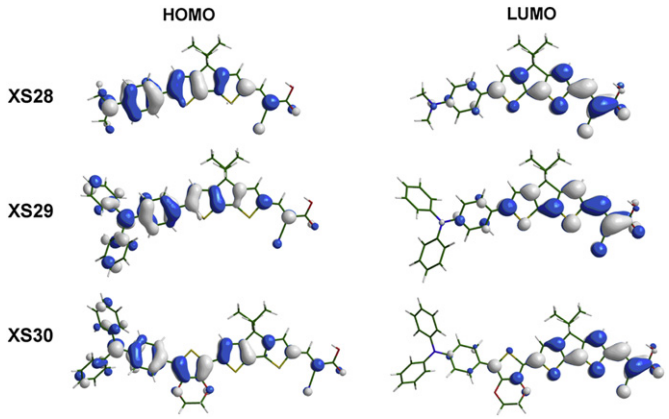

Fig. 3. Isodensity surface plots of the HOMO and LUMO of **XS28**–**30**.

Table 2
Calculated details of electronic transitions with the relative oscillator strengths larger than 0.1 of the dyes.

Dye	State	Calculated energy (eV)	Oscillator strength (*f*)	Transition assignment[a]
XS28	1	2.36	1.08	H → L (78%)
	2	3.15	0.32	H-1 → L (75%)
	3	3.67	0.10	H → L + 1 (69%)
XS29	1	2.22	0.96	H → L (84%)
	2	2.92	0.61	H-1 → L (78%)
	3	3.43	0.15	H → L + 1 (78%)
XS30	1	2.03	1.29	H → L (83%)
	2	2.59	0.66	H-1 → L (80%)
	3	2.96	0.17	H → L + 1 (72%)

[a] H means HOMO, and L means LUMO.

XS28–**30** are −1.23, −1.34, and −1.40 V vs NHE, respectively. Replacement of triphenylamine with *N*,*N*-dimethylaniline shifts the HOMO level negatively and the LUMO level positively, narrowing the HOMO–LUMO energy gaps and resulting in red shift of absorption spectra. Inserting an EDOT unit between the triphenylamine and cyclopentadithiophene shifts the HOMO level negatively due to the electron rich character of EDOT. The LUMO levels for these dyes are more negative than the conduction band of TiO_2 (E_{CB}, −0.5 V vs NHE), which provide sufficient driving forces for electron injection. On the other hand, the HOMO levels for these dyes are more positive than the iodine redox potential (0.4 V vs NHE) [35]. Thus, these oxidized dyes can be regenerated from the reduced species in the electrolyte to give an efficient charge separation. Therefore, the HOMO–LUMO levels of dyes **XS28**–**30** are suitable for DSSCs.

3.3. Photovoltaic performance

Fig. 5 shows the incident photon-to-current conversion efficiency (IPCE) as a function of the wavelength for the sandwiched DSSCs based on the three dyes as sensitizers. The IPCE spectra for **XS28** and **XS30** are broader than that of **XS29**, which is consistent with the absorption spectra of the sensitizers on the similar thickness of TiO_2 films to the DSSCs fabrication condition (Fig. 2b). **XS29** generates high maximum IPCE summit with 84%. Compared with **XS29**, **XS28** with *N*,*N*-dimethylaniline in place of triphenylamine gives lower IPCE with a maximum value of 67%. The IPCE of

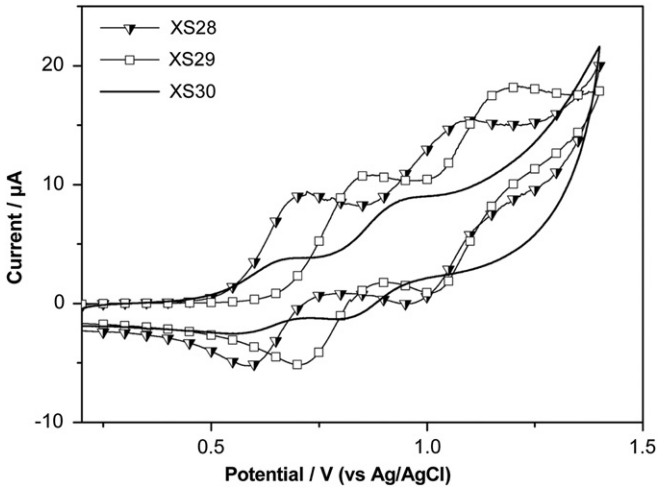

Fig. 4. Cyclic voltammogram of **XS28**–**30** in acetonitrile.

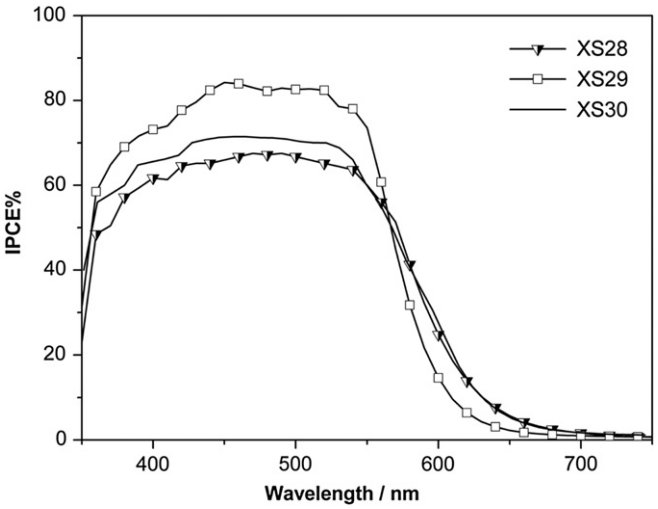

Fig. 5. IPCE spectra for DSSCs based on **XS28**–**30**.

XS30 containing binary conjugated spacer of EDOT and cyclopentadithiophene is evidently lower compared to the **XS29**, which will result in a loss in J_{SC}.

The photocurrent–voltage (J–V) curves for DSSCs based on the **XS28**–**30** are demonstrated in Fig. 6, the corresponding photovoltaic data are listed in Table 3. In agreement with the result of IPCE, the **XS29**-sensitized cell exhibites better photovoltaic performances than those of **XS28**, **30** under standard global AM 1.5 solar conditions. 5.8% of solar energy to electricity conversion efficiency (η) based on **XS29** is achieved with a short-circuit photocurrent density (J_{SC}) of 14.4 mA cm^{-2}, an open-circuit voltage (V_{OC}) of 601 mV, and a fill factor (ff) of 0.67. The power conversion efficiencies (η) for the **XS28** and **XS30** are 4.9% and 5.4%, respectively. In comparison to **XS28**, the efficiency of the **XS29**-based device is somewhat higher due to enhancement of J_{SC} and V_{OC} arising from triphenylamine unit. The efficiency of **XS30** is relative lower than that of **XS29** primarily due to the decreasing of J_{SC}. For a fair comparison, the N719-sensitized TiO_2 solar cell showed an efficiency of 7.9%, with a J_{SC} of 16.8 mA cm^{-2}, a V_{OC} of 695 mV, and a fill factor of 0.68.

Table 3
Photovoltaic performance of DSSCs sensitized with XS28-30.[a]

Dye	CDCA	J_{SC}/mA cm^{-2}	V_{OC}/mV	FF	η/%
XS28	0 mM	12.5	584	0.68	4.9
	1.5 mM	13.7	606	0.69	5.7
	3.0 mM	13.4	598	0.67	5.4
XS29	0 mM	14.4	601	0.67	5.8
	1.5 mM	15.2	605	0.68	6.3
	3.0 mM	15.0	582	0.71	6.2
XS30	0 mM	13.4	595	0.68	5.4
	1.5 mM	14.1	608	0.70	6.0
	3.0 mM	13.2	589	0.72	5.6
N719	N719	16.8	692	0.68	7.9

[a] Photovoltaic performances of DSSCs were measured under irradiation of AM 1.5 G simulated solar light (100 mW cm^{-2}) at room temperature with a 0.16 cm^2 working area. The thickness of the TiO_2 film was 12 μm. Dye bath: ethanol–CH_2Cl_2 3:1 solution (10^{-3} M).

To study the effect of an incorporated ethyl substituted cyclopentadithiophene unit on dye aggregation, the J–V curves of **XS28**–**30** with a variety of chenodeoxycholic acid (CDCA) concentrations are measured (Table 3, Fig. 6b–d). Generally, CDCA is used as coadsorbent to dissociate the π-stacked dye aggregates and improves the electron-injection yield, thus affording higher J_{SC} value [23]. For the three dyes sensitized-DSSCs, the J_{SC} values increase with the addition of CDCA from 0 to 1.5 mM, then decrease with further increase of CDCA (3.0 mM). The results indicate that there was no significant π-aggregation [36] of dyes **XS28**–**30** on the surface of the TiO_2 film, which may be due to the existence of the two ethyl chains on the cyclopentadithiophene unit.

Electrochemical impedance spectroscopy (EIS) analysis is performed to further elucidate the photovoltaic properties. Fig. 7a shows the electrochemical impedance spectra for the DSSCs made with TiO_2 electrodes, dipped with **XS28**–**30** sensitizers under a forward bias of −0.6 V in the dark with a frequency range of 10 Hz to 100 kHz. The larger semicircle at lower frequencies represents the interfacial charge transfer resistances (R_{CT}) at the TiO_2/dye/electrolyte interface. The R_{CT} is related to the charge recombination rate, e.g., a smaller R_{CT} indicates a faster charge recombination. The radius of the larger semicircle increases in the order **XS29** > **XS30** > **XS28**, implying the same order of the electron recombination resistance (R_{CT}) for the three dyes. The electron recombination lifetimes (τ), extracted from the angular frequency at the midfrequency peak in the Bode phase [37] plot Fig. 7b are in the order of **XS29** > **XS30** > **XS28**. These results are in agreement with the observed shift in the V_{OC} value under standard global AM 1.5 illumination. The longer lifetime of **XS29** relative to **XS28** could be attributed to the steric hindrance of bulky triphenylamine unit. Recently, a better correlation was found between electron lifetimes and polarizabilities [38]. In general, organic dyes with high polarizabilities show strong interaction with surrounding species and induce an increase in the local concentrations of acceptor species.

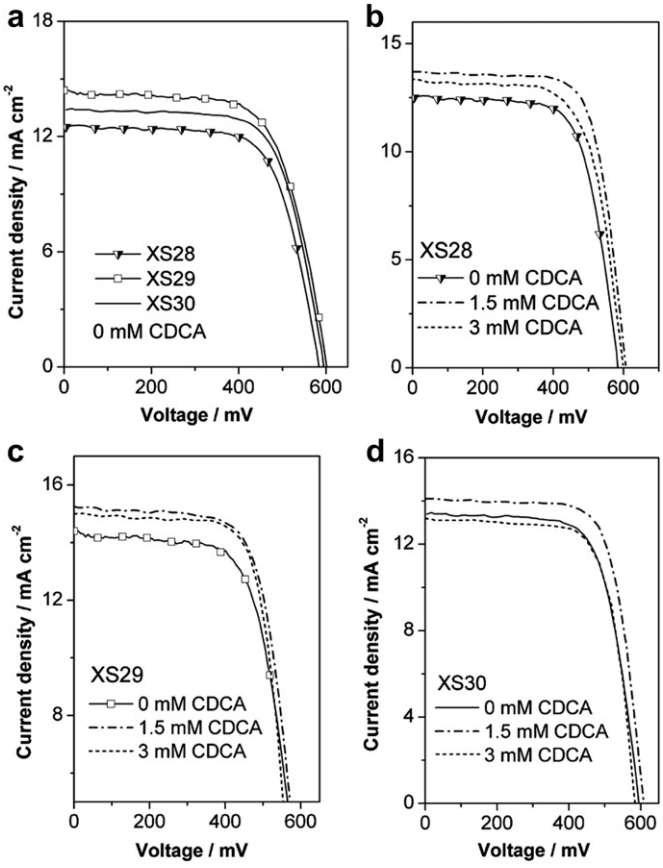

Fig. 6. Current–potential (J–V) curves for the DSSCs based on **XS28**–**30** under AM 1.5 irradiation (100 mW cm^{-2}).

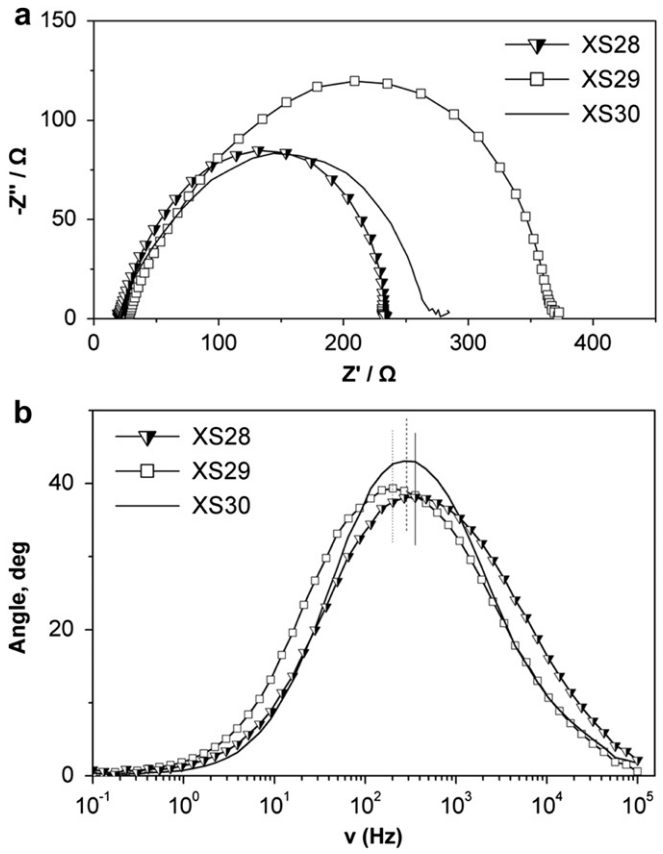

Fig. 7. EIS for DSSCs based on **XS28**–**30** measured in the dark under −0.6 V bias displayed in the form of Nyquist plots (a) and Bode phase plots (b).

Polarizabilities for the **XS28**–**30** were 69, 89 and 119 Å^3, respectively. The shorter lifetime of **XS30** relative to **XS29** may be caused by an increase in the local concentrations of acceptor species due to its high polarizability.

4. Conclusions

In conclusion, three organic sensitizers **XS28**–**30** based on 4,4-diethyl-4H-cyclopenta(2,1-b:3,4-b′)dithiophenes unit were synthesized and successfully used for sensitizing TiO_2 electrodes. The incorporation of an ethyl-substituted cyclopentadithiophene unit as the conjugate bridge shows distinctly characteristics for light-harvesting and efficiency: (i) it exhibits a relatively high molar coefficient in $CHCl_2$ and a notably broad profile upon adsorbtion onto TiO_2 film, which is beneficial for light-harvesting; (ii) it is beneficial to prevent close π–π aggregation, resulting in a high photocurrent. The introduction of the triphenylamine group as the electron-donor brought about improved photovoltaic performance compared with *N*,*N*-dimethylaniline group. Among the three dyes studied, a maximum power conversion efficiency of 5.8% was obtained under simulated AM 1.5 solar irradiation (100 mW cm^{-2}) with a DSSCs based on **XS29** (J_{SC} = 14.4 mA cm^{-2}, V_{OC} = 601 mV, ff = 0.67). These results suggest that the sensitizers based on functionalized cyclopentadithiophene unit are promising candidates for DSSCs.

Acknowledgments

We are grateful to the National Natural Science Foundation of China (21003096, 21072152) and the Tianjin Natural Science Foundation (09JCZDJC24400) for financial supports.

References

[1] O'Regan B, Grätzel M. A low-cost high-efficiency solar cell based on dye-sensitized colloidal TiO_2 film. Nature 1991;353:737–9.
[2] Nazeeruddin MK, Kay A, Rodicio L, Humpbry-Baker R, Miiller E, Liska P, et al. Conversion of light to electricity by cis-X_2bis(2,2′-bipyridyl-4,4′-dicarboxylate) ruthenium(II) charge-transfer sensitizers (X = Cl^- Br^- I^- CN^- and SCN^-) on nanocrystalline titanium dioxide electrodes. J Am Chem Soc 1993;115:6382–90.
[3] Nazeeruddin MK, Zakeeruddin SM, Humphry-Baker R, Jirousek M, Liska P, Vlachopoulos N, et al. Acid–base equilibria of (2,2′-bipyridyl-4,4′-dicarboxylic acid) ruthenium(II) complexes and the effect of protonationon charge-transfer sensitization of nanocrystalline titania. Inorg Chem 1999;38(26):6298–305.
[4] Hara K, Sayama K, Ohga Y, Shinpo A, Suga S, Arakawa H. A coumarin-derivative dye sensitized nanocrystalline TiO_2 solar cell having a high solar-energy conversion efficiency upto5.6%. Chem Commun 2001;6:569–70.
[5] Hara K, Wang Z, Sato T, Furube A, Katoh R, Sugihara H, et al. Oligothiophene containing coumarin dyes for efficient dye-sensitized solar cells. J Phys Chem B 2005;109(32):15476–82.
[6] Seo KD, Song HM, Lee MJ, Pastore M, Anselmi C, Angelis FD, et al. Coumarin dyes containing low-band-gap chromophores for dye-sensitised solar cells. Dyes Pigments 2011;90(3):304–10.
[7] Horiuchi T, Miura H, Sumioka K, Uchida S. High efficiency of dye-sensitized solar cells based on metal-free indoline dyes. J Am Chem Soc 2004;126(39):12218–9.
[8] Ito S, Miura H, Uchida S, Takata M, Sumioka K, Liska P, et al. High-conversion efficiency organic dye-sensitized solar cells with a novel indoline dye. Chem Commun 2008;41:5194–6.
[9] Matsui M, Fujita T, Kubota Y, Funabiki K, Jin J, Yoshida T, et al. Substituent effects in a double rhodanine indoline dye on performance of zinc oxide dye-sensitized solar cell. Dyes Pigments 2010;86(2):143–8.
[10] Matsui M, Kotani M, Kubota Y, Funabiki K, Jin J, Yoshida T, et al. Comparison of performance between benzoindoline and indoline dyes in zinc oxide dye-sensitized solar cell. Dyes Pigments 2011;91(2):145–52.
[11] Tian H, Yang X, Chen R, Zhang R, Hagfeldt A, Sun L. Effect of different dye baths and dye-structures on the performance of dye-sensitized solar cells based on triphenylamine dyes. J Phys Chem C 2008;112(29):11023–33.
[12] Zeng WD, Cao YM, Bai Y, Wang YH, Shi YS, Wang P. Efficient dye-sensitized solar cells with an organic photosensitizer featuring orderly conjugated ethylene dioxythiophene and dithienosilole blocks. Chem Mater 2010;22(5):1915–25.
[13] Li G, Zhou Y, Cao X, Bao P, Jiang K, Lin Y, et al. Novel TPD-based organic D–π–A dyes for dye-sensitized solar cells. Chem Commun 2009;16:2201–3.
[14] Tian Z, Huang M, Zhao B, Huang H, Feng X, Nie Y, et al. Low-cost dyes based on methylthiophene for high-performance dye-sensitized solar cells. Dyes Pigments 2010;87(3):181–7.
[15] Shang H, Luo Y, Guo X, Huang X, Zhan X, Jiang K, et al. The effect of anchoring group number on the performance of dye-sensitized solar cells. Dyes Pigments 2010;87(3):249–56.
[16] Zhang F, Luo YH, Song JS, Guo XZ, Liu WL, Ma CP, et al. Triphenylamine-based dyes for dye-sensitized solar cells. Dyes Pigments 2010;81(3):224–30.
[17] Chen DY, Hsu YY, Hsu HC, Chen BS, Lee YT, Fu H, et al. Organic dyes with remarkably high absorptivity; all solid-state dye sensitized solar cell and role of fluorine substitution. Chem Commun 2010;46:5256–8.
[18] Li R, Liu D, Zhou D, Shi Y, Wang Y, Wang P. Influence of the electrolyte cation in organic dye-sensitized solar cells: lithium versus dimethylimidazolium. Energy Environ Sci 2010;3(11):1765–72.
[19] Liang M, Zong XP, Han HY, Chen C, Sun Z, Xue S. An efficient dye-sensitized solar cell based on a functionalized-triarylamine dye. Mater Lett 2011;65(9):1331–3.
[20] Tian H, Yang X, Chen R, Pan Y, Li L, Hagfeldt A, et al. Phenothiazine derivatives for efficient organic dye-sensitized solar cells. Chem Commun 2007;36:3741–3.
[21] Paek S, Choi H, Choi H, Lee CW, Kang MS, Song K, et al. Molecular engineering of efficient organic sensitizers incorporating a binary π-conjugated linker unit for dye-sensitized solar cells. J Phys Chem C 2010;114(34):14646–53.
[22] Liang M, Lu M, Wang QL, Chen WY, Han HY, Sun Z, et al. Efficient dye-sensitized solar cells with triarylamine organic dyes featuring functionalized-truxene unit. J Power Sources 2011;196(3):1657–64.
[23] Lu M, Liang M, Han HY, Sun Z, Xue S. Organic dyes incorporating bis-hexapropyltruxeneamino moiety for efficient dye-sensitized solar cells. J Phys Chem C 2011;115(1):274–81.
[24] Ning ZJ, Zhang Q, Pei HC, Luan JF, Lu CG, Cui YP, et al. Photovoltage improvement for dye-sensitized solar cells via cone-shaped structural design. J Phys Chem C 2009;113(23):10307–13.
[25] Lin SH, Hsu YC, Lin JT, Lin CK, Yang JS. Isotruxene-derived cone-shaped organic dyes for dye-sensitized solar cells. J Org Chem 2010;75(22):7877–86.
[26] Sayama K, Hara K, Mori N, Satsuki M, Suga S, Tsukagoshi S, et al. Photosensiti- zation of a porous TiO_2 electrode with merocyanine dyes containing a carboxyl group and long alkyl chain. Chem Commun 2000;13:1173–4.

[27] Wang ZS, Li FY, Huang CH, Wang L, Wei M, Jin LP, et al. Photoelectric conversion properties of nanocrystalline TiO_2 electrodes sensitized with hemicyanine derivatives. J Phys Chem B 2000;104(41):9676–82.
[28] Wang ZS, Koumura N, Cui Y, Takahashi M, Sekiguchi H, Mori A, et al. Hexylthiophene-functionalized carbazole dyes for efficient molecular photovoltaics: tuning of solar-cell performance by structural modification. Chem Mater 2008;20(12):3993–4003.
[29] Zhou D, Cai N, Long H, Zhang M, Wang Y, Wang P. An energetic and kinetic view on cyclopentadithiophene dye-sensitized solar cells: the influence of fluorine vs ethyl substituent. J Phys Chem C 2011;115(7):3163–71.
[30] Zhang GL, Bala H, Cheng YM, Shi D, Lv X, Yu QJ, et al. High efficiency and stable dye-sensitized solar cells with an organic chromophore featuring a binary π-conjugated spacer. Chem Commun; 2009:2198–200.
[31] Qin H, Wenger S, Xu M, Gao F, Jing X, Wang P, et al. An organic sensitizer with a fused dithienothiophene unit for efficient and stable dye-sensitized solar cells. J Am Chem Soc 2008;130(29):9202–3.
[32] Mierloo SV, Adriaensens PJ, Maes W, Lutsen L, Cleij TJ, Botek E, et al. A three-step synthetic approach to asymmetrically functionalized 4H-cyclopenta[2,1-b:3,4-b0]dithiophenes. J Org Chem 2010;75:7202–9.
[33] Ito S, Murakami TN, Comte P, Liska P, Grätzel C, Nazeeruddin MK, et al. Fabrication of thin film dye sensitized solar cells with solar to electric power conversion efficiency over 10%. Thin Solid Films 2008;516:4613–9.
[34] Lemaur V, Steel M, Beljonne D, Brédas LJ, Cornil J. Photoinduced charge feneration and recombination dynamics in model donor/acceptor pairs for organic solar cell applications: a full quantum-chemical treatment. J Am Chem Soc 2005;127(16):6077–86.
[35] Hagfeldtt A, Grätzel M. Light-induced redox reactions in nanocrystalline systems. Chem Rev 1995;95(1):49–68.
[36] Li W, Wu Y, Li X, Xie Y, Zhu W. Absorption and photovoltaic properties of organic solar cell sensitizers containing fluorene unit as conjunction bridge. Energy Environ Sci 2011;4:1830–7.
[37] Lagemaat JVD, Park NG, Frank AJ. Influence of electrical potential distribution, charge transport, and recombination on the photopotential and photocurrent conversion efficiency of dye-sensitized nanocrystalline TiO_2 solar cells: a study by electrical impedance and optical modulation techniques. J Phys Chem B 2000;104:2044–52.
[38] Marinado T, Nonomura K, Nissfolk J, Karlsson MK, Hagberg DP, Sun L, et al. How the nature of triphenylamine-polyene dyes in dye-sensitized solar cells affects the open-circuit voltage and electron lifetimes. Langmuir 2010;26(4):2592–8.